Using Inline Digital Holography for Measuring Diffusion of Active Janus Spheres

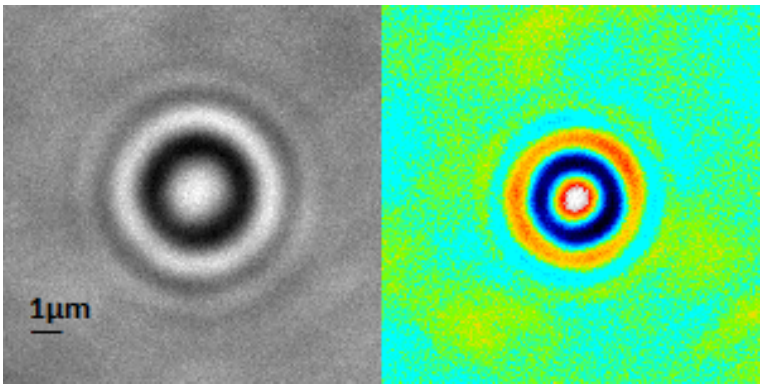

THESIS

submitted in partial fulfillment of the
requirements for the degree of

MASTER OF SCIENCE
in
PHYSICS

Author :	Nick Oikonomeas-Koppasis
Student ID :	1996215
Supervisor :	Dr. D. J. Kraft, R. Verweij
2^{nd} corrector :	Prof.dr. M.A.G.J. Orrit

Leiden, The Netherlands, September 11, 2019

Using Inline Digital Holography for Measuring Diffusion of Active Janus Spheres

Nick Oikonomeas-Koppasis

Soft Matter Group, Leiden University
NielsBohrweg 2, Kamernummer 1005, 2333 CA Leiden, The Netherlands

September 11, 2019

Abstract

We use Inline Digital Holography to measure the diffusion coefficient of spherical colloids with a $1.06\mu m$ radius in the bulk of a liquid. We obtain a diffusion coefficient of $0.23 \pm 0.03\mu m^2/s$ which is in good agreement with Stokes-Einstein theory. We attempt the measurements to active Janus colloid spheres and explore the possibilities and limitations of the technique. We use the Discrete Dipole Approximation to fit the holograms to the Lorenz-Mie theory and report on the viability of the computation. We discuss the minimum necessary requirements for performing a successful fitting and analysis of the motion of Janus colloid spheres, in the bulk of a medium, using inline holography.

Introduction

A colloidal system consists of a mixture of two or more substances mixed together but not chemically combined, such that they can be separated. It is a special type of mixture of particles ranging from a few nm to a few μm in size, dispersed in a medium. In normal solutions, solute and solvent constitute only one phase, whereas in colloidal suspensions there are at least two distinct phases, the dispersed phase and the continuous phase. An everyday example of a colloidal system is cream, which consists of particles of fat dispersed into water. If cream is shaken for a sufficient amount of time, the fat molecules stick together (hence the name colloid from the Greek word "kola" which means glue), and separate the cream into butter and buttermilk. The butter it self is also a colloidal system as there are water molecules trapped between the fat.

Colloidal systems have recently drawn plenty of attention due to their properties. Due to the size of the colloidal particles they can be studied using light microscopy and due to their properties they exhibit behaviors that allow modeling of statistical systems, such as molecules or atoms. There are multiple "dimensions"of the colloidal systems that can be used either for modeling or technological applications, which depend on the number of particles considered and/or their assembly interactions. For example, we can study phase behavior [1, 2], packing, topology, or entropy effects[3] since the individual particles are small enough to be sensitive to thermal fluctuations [4]. In addition, colloidal particles have recently emerged as a pivotal point of interest in Biological systems. Red blood cells is a good example of a colloidal biological system of great interest [5].

A special case of colloidal particles are active colloids. Activity can be induced in different ways, but in this particular project we discuss Janus spheres. When one hemisphere is coated with a metal that can catalyse a fuel, in our particular case, Platinum, which catalyses hydrogen peroxide(H_2O_2), the sphere acquires a self-propelling mechanism. Due to the half coating the spheres are referred to as Janus spheres, taking their name from the Roman god with two faces. Janus particles have been used as building blocks in multiple fields. With the rising interest in active matter physics they have been used as probes for colloidal assemblies [6], but have also seen applications in medicine as smart drug delivery devices [7].

The activity of the Janus particles has been studied in a quasi-2D environment in multiple conditions. Surface-particle interactions are being studied continuously [8, 9] and has seen rapid development both in modeling and experimental work. However, motion in 3D is poorly understood, partly due to the difficulties presented by 3D microscopy and partly due to the strong affiliation of active particles with the surface. Particles in the bulk of the medium do not experience interactions with surfaces, reducing the open parameters of the description of their motion. In the absence

Version of September 11, 2019– Created September 11, 2019 - 11:12

of surface interactions we can obtain a pure description of the diffusion and activity of the particles. This can serve both as a building block for more complex interaction, i.e. collections of active particles in the bulk, and as a disentanglement tool of the active and diffusive components motion and the surface interaction when the particles are studied in a quasi-2D environment. Finally, complex real systems such as the red blood cells mentioned above, require a 3D description to be fully understood.

Digital holography, though it was developed in the early 70's, has only been employed for tracking measurements recently as it carried a heavy computational load. Recent development in digital inline holography[10] and the increased interest for tracking and characterizing colloidal particles have created a fertile ground for use of this technique for 3D tracking. Holography is a technique based on the Lorenz-Mie scattering theory, which describes the diffraction pattern produced when light passes through a small transparent sphere.

Unlike traditional light microscopy, in digital holography we collect information about the intensity interference pattern of the light at the focal plane. The pattern which is described by the Lorenz-Mie theory, depends on a series of parameters, including the height of the particle from the focal plane (see Theory). We can reproduce a model through a numerical fitting that will also depend on the same parameters and match it with the recorded data to obtain the 3D location of a sphere with respect to the focal plane.

Through this technique we are able to reconstruct the 3D trajectory of a particle. The main aim of this project is to obtain a diffusion coefficient for particles diffusing in the bulk, i.e. not interacting with the substrate, for both passive colloidal spheres and active Janus spheres. By minimizing the interaction with external factors, it is possible to look at individually to Brownian motion, motion due to activity, and motion due to gravity. Disentangling the components of the motion will allow us to have a full description of the behavior of the active particle in the bulk of the liquid. Since the disentangled components can be attributed to different mechanisms, the individual mechanisms that induce that component of the motion can be studied.

Theory

Diffusion and Sedimentation

To study the 3D motion of Brownian particles we can study their diffusion. To correctly describe the process it is important to consider two individual contributions to the motion of a particle, the Brownian motion and the motion under the effect of gravity. Diffusion is a process by which molecules or particles become evenly distributed across a medium. Brownian motion is the result of constant bombarement by the mediums molecules on the particle. When there is a concentration gradient of particles, the statistically uneven bombard-

Version of September 11, 2019– Created September 11, 2019 - 11:12

ment from the high concentration side results in a net flow of the particles towards the lower concentration regions, diffusion. Measuring the net flow in the form of mean square displacement, we can measure the rate at which a particle diffuses over time, the diffusion coefficient D, which is determined by the nature of the system of medium-particle.

We start with the simplest case of a uniform sphere of constant density ρ_0 diffusing freely in a medium with dynamic viscosity η. The diffusion coefficient, under the no-slip condition as predicted by Stokes-Einstein, can be calculated by:

$$D = \frac{k_B T}{6\pi\eta\alpha} \tag{1}$$

where α is the radius of the sphere, T is the temperature,k_B is Boltzmanns' constant and η is the dynamic viscocity of the medium.

To incorporate the gravitational contribution to the motion we first consider the buoyant mass:

$$m_b = m_0(1 - \frac{\rho_f}{\rho_0}) \tag{2}$$

where ρ_f is the density of the fluid and the subscripts b and 0 denote the buoyant mass and the rest mass respectively. An isolated sphere that satisfies the no-slip condition, sediments under the effect of gravity at an average Stokes velocity:

$$u_{Stokes} = \frac{m_b g}{6\pi\eta\alpha} \tag{3}$$

We can now define two relevant time scales, the Brownian time it takes for the particle to diffuse one radius:

$$\tau_B = \frac{3\pi\eta(2\alpha)^3}{4K_B T} \tag{4}$$

and the time that it takes the particle to sediment one radius:

$$\tau_S = \frac{\alpha}{u_{Stokes}} \tag{5}$$

From the two relevant time scales we can obtain the Peclet number:

$$Pe = \frac{\tau_B}{\tau_S} \tag{6}$$

which can intuitively be interpreted as a measure of the relative contributions of gravity and Brownian motion to the particles total motion. In this thesis the Peclet numbers of various particles used for experiments where calculated to be in the order of 10, indicates a tenfold stronger contribution of gravity to the motion of the particle compared to Brownian motion.

Experimentally we can calculate the diffusion coefficient by plotting the mean square displacement (y axis) against lag time (x axis). The mean squared displacement of a given lag time averages over the square of all difference of all pairs of positions spaced by that time, thus calculating the displacement not based on absolute positions but relative to the previous one. When enough pairs are considered, random effects cancel out. Considering multiple lag times we can distinguish three cases. If the plot is linear the particle is purely diffusing, if it is increasing with a power greater than 1 then there is

Version of September 11, 2019– Created September 11, 2019 - 11:12

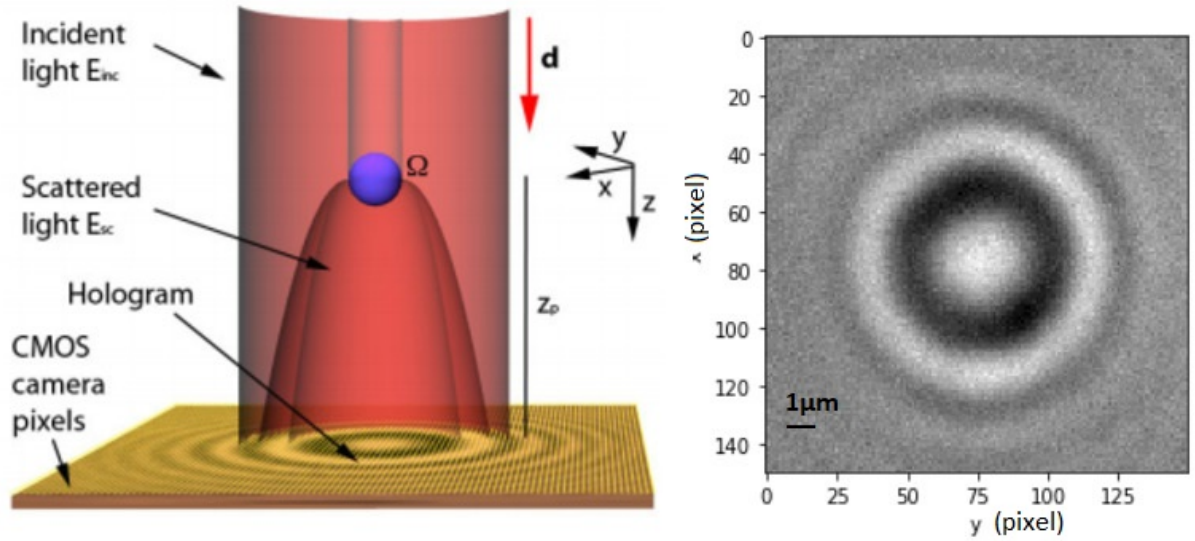

Figure 1: *(left) A schematic of the experimental set-up used for in-line digital microscopy. The incident light with intensity E_{inc} is scattered by an object, resulting in the scattering pattern following the Lorenz-Mie theory. Schematic taken from Dimiduk et. al. 2013. [10].(right) An example of a hologram produced by a silica sphere of radius α=1.06 μm. The position and intensity of the fringes reveal information about the 3D position with respect to the focal plane.*

an additional mechanism contributing to the motion, for example active particles catalysing fuel faster on the coated face, and if it is less than 1 the particle is constrained. For a particle whose motion is attributed solely on Brownian motion:

$$\left\langle \Delta r^2 \right\rangle = 2NDt \tag{7}$$

where N is the number of dimensions (every dimension contributes $2D$ to the slope).

Holography

Holographic microscopy allows for the extraction of information about the 3D position of a scattering object through digital reconstruction of the hologram. A coherent, monochromatic source of light passes through a scatterer and the interference pattern is captured at the focal plane. A simple schematic of the set-up used is illustrated in *Figure 1* on the left side, offering a simple view of how the diffraction pattern is formed. On the left is an example image produced by a silica sphere at a height of 15 μm with respect to the focal plane.

The incident plane wave with known reference field E_{ref} interferes with the scattered field E_{scat} and combines to form the hologram described by:

$$\mathbf{H}(\mathbf{s}, n, r, a) = \left| aE_s(\mathbf{s}, n, r) + E_r \right|^2 \tag{8}$$

where **s** is the positional vector in 3D, n is the refractive index of the scatterer, r

Version of September 11, 2019– Created September 11, 2019 - 11:12

its radius and α is rescaling of the scattered field and it is poorly understood [10, 11]. H denotes a matrix of intensities with elements (i,j) corresponding to pixel intensity in the recorded image. Following closely previous work [11] we arrive at the normalized hologram expression:

$$\mathbf{h} = \frac{\mathbf{H}(\mathbf{s}, n, r, a)}{|E_r|^2}$$

$$= \left| \frac{aE_s(\mathbf{s}, n, r)}{E_r} + 1 \right|^2 \qquad (9)$$

Since the reference wave intensity, E_r, is known and the normalized hologram, h, is calculated from the captured image, fitting of the scattered intensity, E_s provides the parameters that solve the system of equations.

The pattern described by the Lorenz-Mie scattering theory consists of a series of fringes alternating with radial symmetry (for a sphere) from local maxima to local minima[12]. The light will travel different paths within the scatterer and after exiting. When it arrives at the focal plane it will constructively (maxima) or destructively (minima) interfere based on the distance traveled. In the case of the sphere, a bright spot will always appear in the middle as the incoming light will create a series of focii along the axes that passes through the center and is perpendicular to the focal plane[13]. The theory does not hold when the focal plane is close ($5\mu m$) to the scatterer.

Janus Particles

The term Janus Particles in a scientific context was coined by Ondarcuhu et. al (1990)[14] discussing the properties of amphifilic particles at fluid interfaces, although a similar system was studied by De Gennes earlier. The catalysis of hydrogen peroxide (H_2O_2) by Platinum (Pt) was first explored as a self-propulsion mechanism by Ismagilov et. al. (2002)[15]. Spattering colloidal spheres with a thin film of Pt and placing them in an H_2O_2 suspension allows the particles to self-propel.

To induce propulsion we must break the symmetry of the particle, either by changing its shape or by changing its properties on part of the particle[16]. The Janus particles we use self-propel through catalysis and perform active Brownian motion, along the gradient of the fuel concentration. We thus expect that if we measure the mean squared displacement for such particles in the presence of fuel we will observe a non-linear graph, but a scaling with a power greater than 1 instead.

Method

Sample preparation

Two types of particles were used throughout our experiments, with radii $1.06 \pm 0.03\mu m$, and synthesized from silica, and 3-methacryloxy-propyl-trimethoxysilane (TPM). The samples underwent a cycle of three washes with miliQ (ultra-purified water) of 5

Version of September 11, 2019– Created September 11, 2019 - 11:12

minutes each to clean the surface of the particles and then a sonification bath for 30 minutes to reduce aggregation. The stock of particles was concentrated to 5% weight to volume. We first diluted $50\mu L$ in 1mL of miliQ which we used as stock for sample preparation. We further diluted the latter 1000times with miliQ to a total dilution of 0.000025% weight to volume. Sufficient dilution is essential as it ensures that the particles are sufficiently isolated. Isolation is necessary because particles that are close to each other create overlapping diffraction patterns, and are not possible to analyze.

We placed the diluted samples in a round sample holder with 2mm depth, flipped the holder so that the particles reached the upper cover slip under the effect of gravity and let the sample rest for 20 minutes. The samples were flipped again and put on the microscope. We focused on the lower cover slip and then the focal plane was moved 1mm up to capture the sedimenting particles. For correctly analysing the captured images it is essential that the focal plain is sufficiently away from the height of the particles center as close to the focal plane near field effects take over and the Lorenz-Mie theory does not adequately describe the scattering. It is not an easy task to accurately quantify exactly the cross-over between the near field and far field regions, however it is also not essential for the purpose of our experiments. The only requirement is to stay sufficiently above (or below) the cross over height. We empirically determined that at $5\mu m$ distance from the focal plane the fitting is always possible.

Microscopy

We followed an identical procedure for all data collected and discussed in this thesis which was determined based on maintaining the best quality of data whilst keeping the computational requirements within the scope of our technical capabilities. The computational difficulties will be discussed briefly in the next section and extensively in the Discussion section.

A 660nm LED light source was used as the incident light. The light was linearly polarized as it allows for sharper images and better description of the incident beam[17]. All images were collected with an Extra Long Working Distance(ELWD) 60X Air objective and numerical aperture (NA) of 0.70 , on an Nikon Ti-Eclipse microscope, and recorded with a DS-U3 Nikon digital camera. Before collecting data we performed a Köhler illumination with a 20X objective, NA 0.75, and then with the 60X Air objective using a Brightfield lamp. We switched the light source to the LED and, prior to recording, the objective was moved out of focus and three reference images were taken to perform a background correction. An image with the light source switched off is required, which is referred to as a darkfield image by the Holopy library (though does not correspond to darkfield microscopy). The darkfield image corrects further for noise in our system

produced by external sources. These are essential steps as they reduces the amount of interference from foreign objects that can overlap with the hologram and create inconsistencies. Before recording data it is important to verify that a single sphere is being recorded, as at large heights the set-up that we used does not efficiently resolve the difference of small clusters of spheres and single spheres. To achieve that we focus on the particle chosen before moving the objective sufficiently away to record the data.

Analysis

For the analysis and fitting of the holograms we follow closely the work of Dimiduk et. al. (2016) [18] which will be outlined here. For a more detailed understanding refer to Appendix I. The analysis and fitting has been implemented in a complete, open source python library, Holopy, with extensive documentation and tutorials. The Holopy library uses a Bayesian interference approach to solve the problem. The scattered field, E_s, can be calculated based on the posterior probability (hence, *posterior*): the probability distribution of the parameters that define it, based on the data collected. To consider the posterior we first need to describe the noise in our recorded hologram which as discussed in previous work [11, 18] can be due to photon shot noise, electronic readout noise, and fringes due to foreign objects in the optical train. With very careful preprocessing of the images we can eradicate the later, therefore only the prior two noise sources are implemented in the analysis. The hologram recorded can be then expressed as the sum of equivalent model and the noise at each pixel:

$$h_{ij} = h_{ij}^{M} + u_{ij} \tag{10}$$

where h_{ij}^{M} indicates the forward model of the hologram, with i, j the matrix elements as defined by equation (8), and u indicates the noise at each pixel.

Two types of analysis can be performed, one where the particles' properties are characterised (n and r), and one where the particles position is tracked. We are interested in the later. We used particles where the radius and refractive index is well known (this was not the case for the coated spheres) and were confined parameters within tight upper and lower bounds. As formulated by *Dimiduk et. al. 2016*, [18] we can write the marginalized distribution for the particle tracking as:

$$p'(\mathbf{s}|\mathbf{h}, M, I) = \int d\mathbf{s}\, d\alpha\, p'(\mathbf{s}, n, r, \alpha|\mathbf{h}, M, I) \tag{11}$$

where p' is the unnormalized posterior probability distribution, $\mathbf{s}$ is the positional vector, and M is the forward model. Equation (11) is the analytical expression for evaluating the best fit based on the unbound parameters, and I denotes the priors information which will be discussed in detail in the following paragraph. The integrals however, cannot be solved analytically. Due

Version of September 11, 2019– Created September 11, 2019 - 11:12

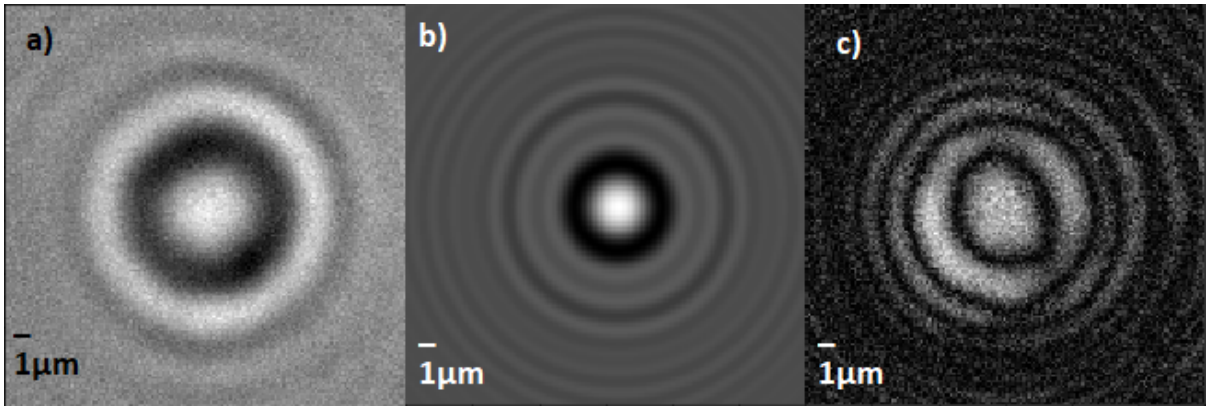

Figure 2: *a) Recorded hologram of a TPM particle with radius of* $1.06\mu m$ *radius. b) The fitted model calculated by Holopy for the same particle. c) The residual intensity after subtracting the model from the data. It becomes clear that the model is not converging to the correct parameters for the fitting. We observe a consistent trend of divergence between the model and the data.*

to the number of parameters, a brute force computational approach for obtaining results is not possible. In practice therefore, a Markov-Chain Monte Carlo (MCMC) technique is employed to numerically solve the integral[19].

Before performing the MCMC we can provide a series of priors, either bound or unbound, which represent our knowledge of the holograms parameters. In practice, in the tracking characterisation of a particle, if the radius and the refractive index are well known, we can obtain the x and y location of the center of the hologram using a circle transform due to its symmetry with sub-pixel accuracy, leaving only the z position and the parameter α open. The latter is always bound between 0 and 1 and a good and rather conservative estimate would be between 0.5 and 0.9. The height becomes the main parameter we aim to obtain from the analysis. If we leave the parameter completely open for fitting, the computational time becomes extremely large, about 45 minutes per frame.

To approach the problem we chose to perform a robust analysis on the first frame to obtain a good first position and then feed it as a prior to the next frame. In this way, we were able to reduce the time of subsequent frames to 2 minutes per frame and still obtain good results. To perform the fitting we use an affine invariant ensemble sample provided by the emcee Python library [19, 20]. The technique is extensively documented so we will focus on the optimization process we followed for obtaining results.

The initial frame was corrected by a background image and a dark-field image. The center of the x-y plane was calculated with a circle transform and fed as a prior to the model with a two pixel standard deviation (the prob-

Version of September 11, 2019– Created September 11, 2019 - 11:12

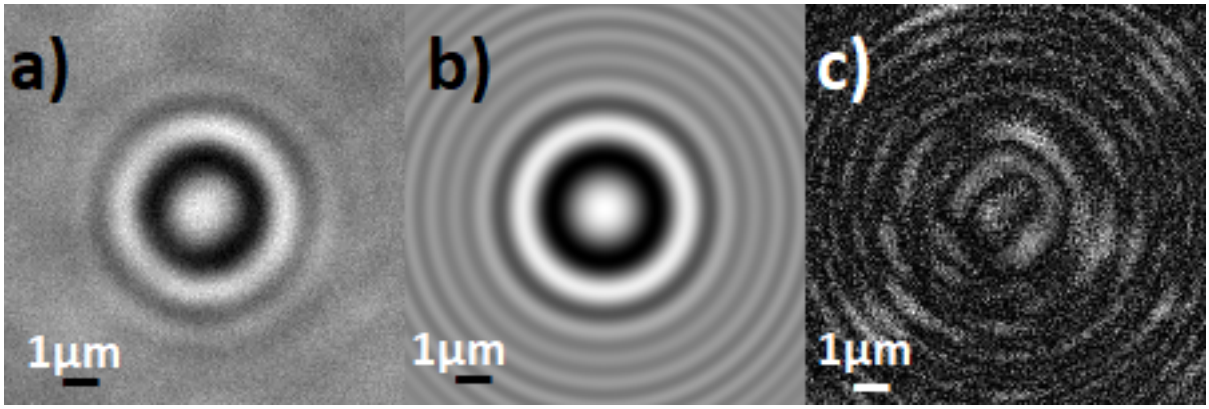

Figure 3: *a) A normalized experimental hologram, b) the fitted model and c) the residual hologram. The intensity of the residual has been amplified by a factor of 10, indicating that the brightest spots represent a fractional intensity difference of 0.1 with respect to the data.*

ability is Gaussian distributed). The radius of the silica particles was obtained from the manufacturing specification and was given the quoted error as bounds for the prior. The same was done for the refractive index. For TPM however, the refractive index has been previously measured [21, 22] but we consistently observed a divergence of the model when analysing TPM particles and chose to not collect data using them. *Figure 2* shows an example of the divergence of the model for a TPM particle. Immediately it becomes apparent from *Figure 2* that the model does not match the data, and the parameters obtained as a result of the fitting cannot be trusted. The asymmetry in the residual image is a direct result of the bad fitting and the noise in the data.

The fitting of the model is performed by a series of walkers which perform initially a random walk in the parameter space and then eventually converge to a value of each parameter. The walk is either bound to an upper and lower limit or unbound, defined by the initial priors that are given as a starting point. The pixels of the data hologram are sampled randomly and a fitted model is cross-checked with the samples considering the matching of intensity between the model and the data. A robust fitting of the first frame was done by sampling a random subset of 1/4 of the hologram by 500 walkers per parameter and 1000 sampling cycles. Subsequent frames were sampled at a 0.1 fraction of pixels, 100 walkers and 300 sampling cycles. Compared with the original work by *Dimiduk et. al.* (2016)[18], we sample a larger fraction of pixels, compared to their sampling of 1/10 of the total pixels of the initial frame. This is required in our case because we resolve less fringes compared to their data.

It is essential to use tools with which we can check the quality of our fit-

Version of September 11, 2019– Created September 11, 2019 - 11:12

ting. The first such tool is the calculation of the residual image when the model hologram that has been fitted is subtracted from the data as shown in *Figure 2 and 3 c)*. For illustrative purposes the intensity of the residual image has been amplified by a factor of 10. Net intensity differences between the model and the data can be accounted for by the parameter α discussed previously. Though important to resolve, the effect of this parameter corresponds more to the optical train of the set-up rather than the physical parameters of the hologram [10]. We noticed no increase in the error of subsequent frames when reducing the number of pixels sampled, the steps and the number of walkers of the fitting since the priors where adapted based on the acquired information from the first frame and allowed for an equally accurate and faster fitting.

A second tool that was employed to check the quality of the fitting is the acceptance fraction, α_f, which quantifies the number of proposed steps taken by the walkers that are accepted [20]. It ranges between 0 and 1, and can be interpreted as follows: Values close to 0 correspond to very few proposed steps accepted, thus the chain has a low number of independent samples and therefore is biased. Values close to 1 mean the majority of steps are accepted and the chain is performing a truly random walk, independent of the target (data). A value indicating that the fitting was correct and unbiased falls in a range from 0.2 to 0.5 [10, 20].

To calculate the diffusion coefficient for long time diffusion of the particles used we measured the mean square displacement over a lag time of one second, sufficiently longer than the Brownian characteristic time scale [23] , defined by:

$$\tau_{ST} = \frac{m_b}{6\pi\eta r} \tag{12}$$

where the ST subscript stands for short-time, and m_b is given by equation (2). For the particles used in our experiments, τ_{ST} is 0.46μs.

The diffusion coefficient along each direction axis should remain constant. However, we have to account for the motion due to gravity on the z-axis, and a certain amount of drift in our sample. To achieve that we add a term to equation (7) and rearrange so that the slope still represents the diffusion coefficient. Along each axis equation (7) becomes:

$$\left\langle \Delta r^2 \right\rangle - u^2 t^2 = 2NDt \tag{13}$$

where u is the average velocity along each axis, calculated by plotting position vs time and obtaining the slope. Through careful sample preparation we managed to keep u_x and u_y at a minimum, corresponding to a minimum amount of drift. It is worth mentioning that this is not the best possible solution to account for drift, however the robust approach for subtracting drift which requires analysing multiple particle trajectories and averaging over them is not possible in our case. We will see in the results section that this approach does not affect negatively the quality of our data.

Version of September 11, 2019– Created September 11, 2019 - 11:12

Error considerations

Beside the measurement noise it is fundamental to discuss errors that arise from the analysis of our data. For known properties such as the radius of the particles and the known refractive indexes we used the spread provided by the manufacturer, and will be stated explicitly in the results section. For calculating the the characteristic values from equations (1) to (6) the error was propagated by standard error analysis.

We set a series of quality controls chosen empirically to define a crude acceptable fit from the analysis. Acceptance fractions exceeding or below the accepted values resulted in an immediate rejection. In addition, no fitting was considered sufficiently good if the intensity maximum of the residual image exceeded 20% of the data maximum intensity. After those two conditions were satisfied the model was considered a good fit. The parameters are given as maximum likelihood value with a standard deviation as its error, calculated by the convergence of the walkers that performed the random walk of this parameter. The given likelihood ignores the first portion of the random walk which is the equilibration time, shown by the red vertical line in *Figure 4*. As an example, *Figure 4* illustrates the random walk in the parameter space. It becomes clear from the figure that the well known position of the x center (left) converges into a sharp "peak" while z center (right) has a broader terminal points for the walkers. The y-axes in *Figure 4* both span 2μm. The distribution of the arrival points is not necessarily symmetric as shown in *Figure 5*, which results to asymmetric errors defined by the number of walkers that arrived above or below the mean value. The final arrival points of 200 walkers is unevenly distributed with a skew of -0.59 indicating a preference above the mean. To ensure this in not a purely statistical effect, every step after equilibration is taken into account. Compared to the x and y center errors, the fitting error for the z center is an order of magnitude larger, which when propagated for any further consideration dominates even more. For that we can consider the error in the x-y location of the center negligible in comparison.

We handled the asymmetry in the z location error by always considering the largest value of the two as a $\pm$ symmetric error, which though not optimal, had a negligible effect in the overall errors of the diffusion coefficients calculated. We note that there are cases were a walker can get "trapped" in a path which is considerably away from the convergence point and yield an enormous error. In those cases, we repeated the analysis, providing different priors, with smaller standard deviation, based on the previous chain. This consistently eradicated the problem of the stuck walkers which were producing an incorrect local maximum in the posterior probability and produced models in good agreement with the data.

Based on our light source and the objective used, we did not manage to reach the accuracy of a few nm quoted in previous work [10, 24]. We can confidently

Version of September 11, 2019– Created September 11, 2019 - 11:12

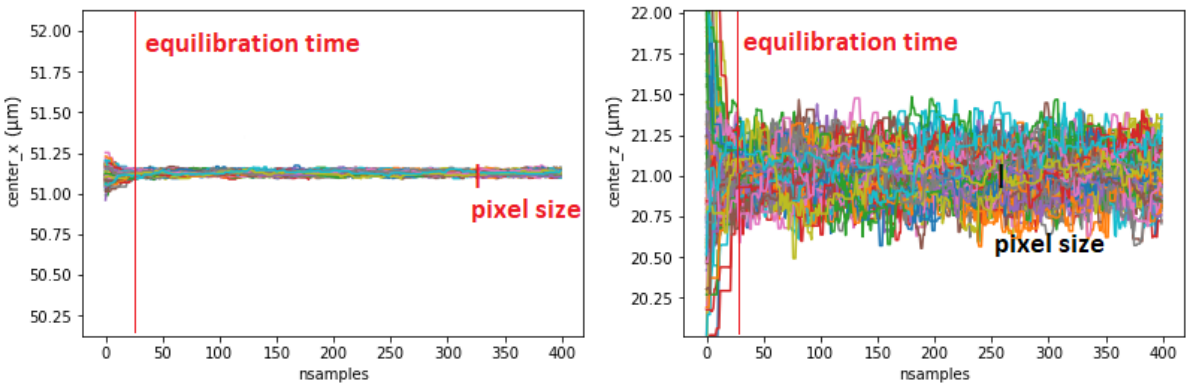

Figure 4: *The random walk performed in the parameter space to converge on the x-axis location of the center. The walkers quickly converge to an almost single value with sub-pixel accuracy. (Right) The random walk of the same hologram in the z-axis location. The walkers still converge to a value however the spread of the values is almost 0.5µm. Both y-axis of the graph span 2µm and the equilibration time is shown as the a red vertical line.*

state that the z positions obtained are correct within a few hundred nm. We believe the main reason for that is the spatial coherence of the light source as the number of fringes we are able to distinguish and therefore use as our raw data for fitting is significantly less compared with data published in previous tracking papers. This is discussed in depth by Deng et. al (2017) [25] and remained a constraint throughout our experiments. Finally, it is important discuss the errors in the calculation of the diffusion coefficient given by the mean square displacement fitting. It is perhaps not straightforward how the errors are calculated as the standard localization error does not suffice [26]. To that we recognize three individual points to discuss: the localization error, the number of points at each lag time interval, and the fitting error. The localization error is directly considered and calculated in each pair by propagation. Secondly, we chose a maximum lag time of 1s, which allowed us a minimum of 10 pairs per point, to obtain a statistically valid sample. Lastly, we obtain an error from the fitting, after anchoring the y-intercept at 0 as it is physically required. The main uncertainty in the experimentally measured coefficient comes from the uncertainty in the z position as will be shown in the Results section.

Results

Sedimentation of passive colloids

We started our experiments with the sedimentation of passive colloids to serve both as a comparison measure with the active colloids as well as to check that the analysis scripts that we

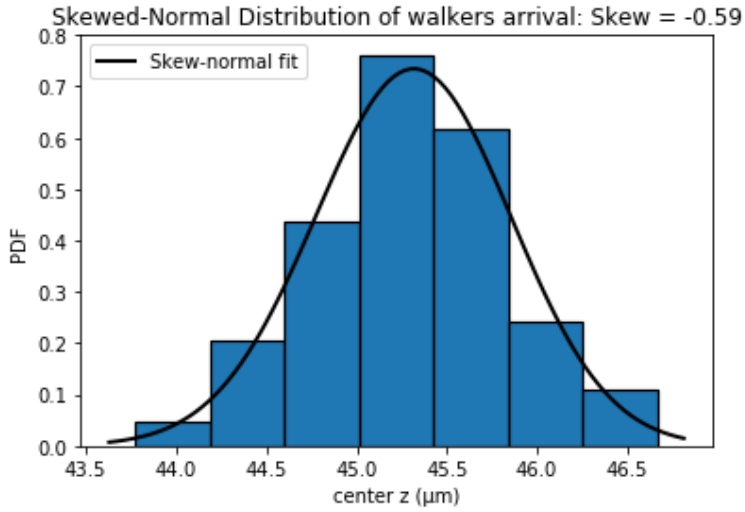

Figure 5: *Arrival point distribution of 200 walkers walking in the z-parameter space. The distribution is not normally distributed around the mean but has a slight preference for values above the mean, represented by the skewness value which is -0.59. A value for skewness equal to 0 represent a normal distribution.*

have written worked correctly. We used silica particles of radius $1.06 \pm 0.03 \mu m$ The imaging was done with 60X objective, NA of 0.7, and 0.09μm/pixel magnification. In *Figure 6* the random walk performed by the walkers converges quickly to the correct value and with a spread of 50nm, which was within the 10% error provided by the manufacturer.

The refractive index was expected to be 1.43 . In the same characterization we obtained a value in good agreement as shown in *Figure 7*. To verify the characteristics and the consistency of the analysis we recorded a 300 frames movie of a stuck particle. We then repeated the characterization for each frame with unbounded priors. The result remained consistent for each frame as shown in *Figure 8*. We hence calculated the average of the radius and the refractive index over the 100 frames and used that value as a known parameter for any subsequent analysis that follows. The value obtained was $1.058 \pm 0.005 \ \mu m$, in which case the error contribution can be considered negligible and doesn't need to be considered in the propagation when calculating the diffusion coefficient. Similarly the refractive index was calculated to be 1.431 ± 0.003, and also does not contribute significantly to the calculation of the errors later on.

We tracked the sedimentation of three separate particles in water. We used the same silica particles that were characterized to minimize our open parameter. The tracking was done over 300 frames, with 10 frames per second imag-

Version of September 11, 2019– Created September 11, 2019 - 11:12

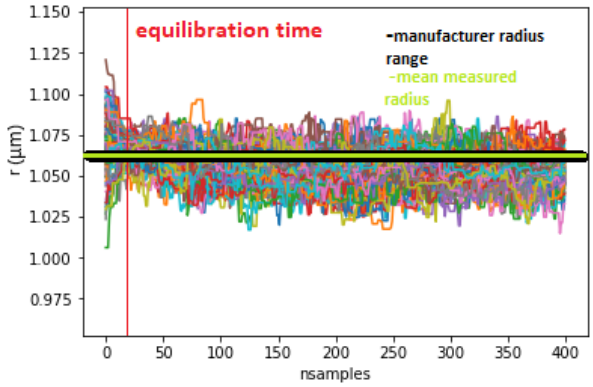

Figure 6: *Convergence of walkers to the expected value of 1.06μm, for the silica particles. The characterization of the particles radius was done within 50nm accuracy, well within the 10% error provided by the manufacturer. Characterization was done with sub pixel accuracy.*

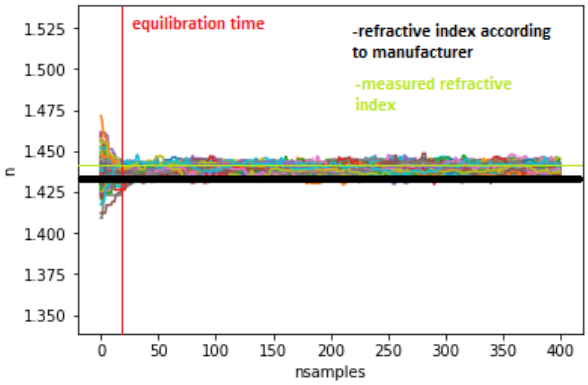

Figure 7: *Convergence of walkers close to the expected value of 1.43 for the refractive index, for the silica particles. The value is in good agreement with that quoted by the manufacturer and the spread given by the fitting is of the order of 0.01, negligible for the purpose of our experiments.*

ing speed, out of which the first and last 130 frames were used, such that the movie was split in two. We chose to do this because during the sedimentation the particle came in focus and hence sedimented away from the focal plane. Whilst the particle is in focus it can not be correctly analysed as explained in the Method section of this report, forcing us to discard 40 frames. We note that the diffraction pattern does not depend on whether the particle is below or above the focal plane and the analysis only reveals a height distance from the focal plane, either above or below. Thus, we treated each 130 frames movie as a separate trajectory of the same particle.

We tracked each pair of trajectories in the bulk of the medium and plotted each component of the motion individually. We performed a linear fit in all three directions in order to correct for the drift and gravitational component of the motion as described in equation (13). For silica particles with radius of 1.06μm and density $\rho = 1.85 g/cm^3$, in water with dynamic viscosity $\eta = 1.0005 g/ms$ and density $\rho_f = 0.998 g/cm^3$ the expected Stokes velocity is equal to $2.1 \mu m/s$. After averaging over all the trajectories analysed, we obtained a value for the Stokes velocity as:

$$u_{ST} = 2.01 \pm 0.01 \mu m/s$$

which is slightly lower compared to the theoretical prediction. Small variations in the radius, temperature, and the mass, as well as hydrodynamic effects that we have neglected should account for the discrepancy.

Version of September 11, 2019– Created September 11, 2019 - 11:12

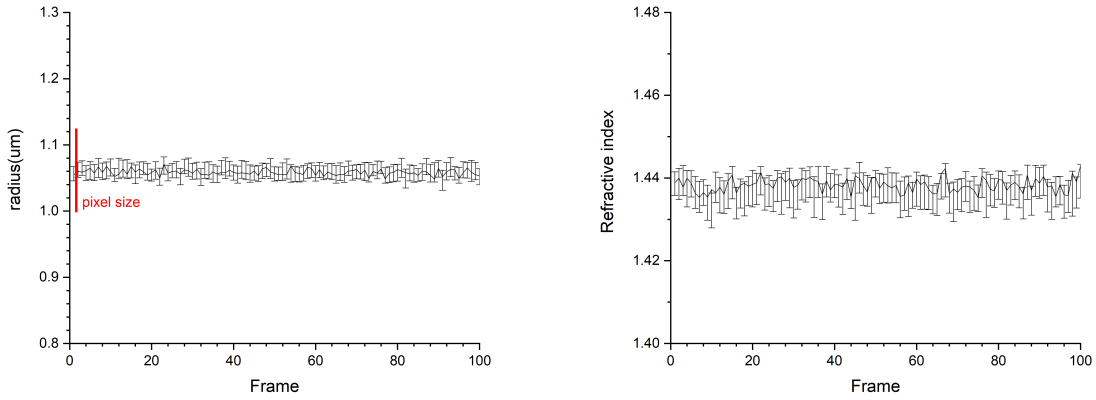

Figure 8: *(Left) Characterization of the radius of a silica sphere expected to have a radius of* $1.06\mu m$*. The sphere is stuck at the substrate hence its x-y-z position is fixed. The analysis is done over 100 frames. (Right) Characterization of the refractive index of the same sphere. The fitting yields results in good agreement with the specifications of the manufacturer and is consistent over the length of the movie.*

In *Figure 9* an example of a tracked trajectory is shown. The focal plane is below the particle, hence the particle's separation is reducing over time. We fitted a linear function to the trajectory taking into account the uncertainty in z. *Figure 10* below shows the 3D trajectory of the particle as it sediments over time. The positions taken are the mean position and error bars are omitted for the sake of clarity. Gravity dominates the motion of the particle, as the Peclet number is 11.

The drift velocities measured for the x and y component of the motion varied between samples. It is worth mentioning, however, that we did not observe velocities above $0.3\mu m/s$, and hence we believe that this type of correction does not bias our results. In addition, these velocities are an order of magnitude smaller than the Stokes velocities, so when considering the 3D diffusion their contribution is further diminished.

From the Stokes-Einstein equation (1) we calculated the diffusion coefficient predicted for the silica sphere to be equal to:

$$D = 0.206 \pm 0.004\mu m^2/s$$

The diffusion coefficient is given for a range of temperatures between 20 and 30^oC because the temperature of the sample changes as it heats up from the light source. We point at the fact that the diffusion coefficient is calculated under the no-slip condition. In addition, a certain measure of drift that is inevitably present will result in an increase in the measured diffusion coefficient.

We calculated the mean square displacement on each component of the

Version of September 11, 2019– Created September 11, 2019 - 11:12

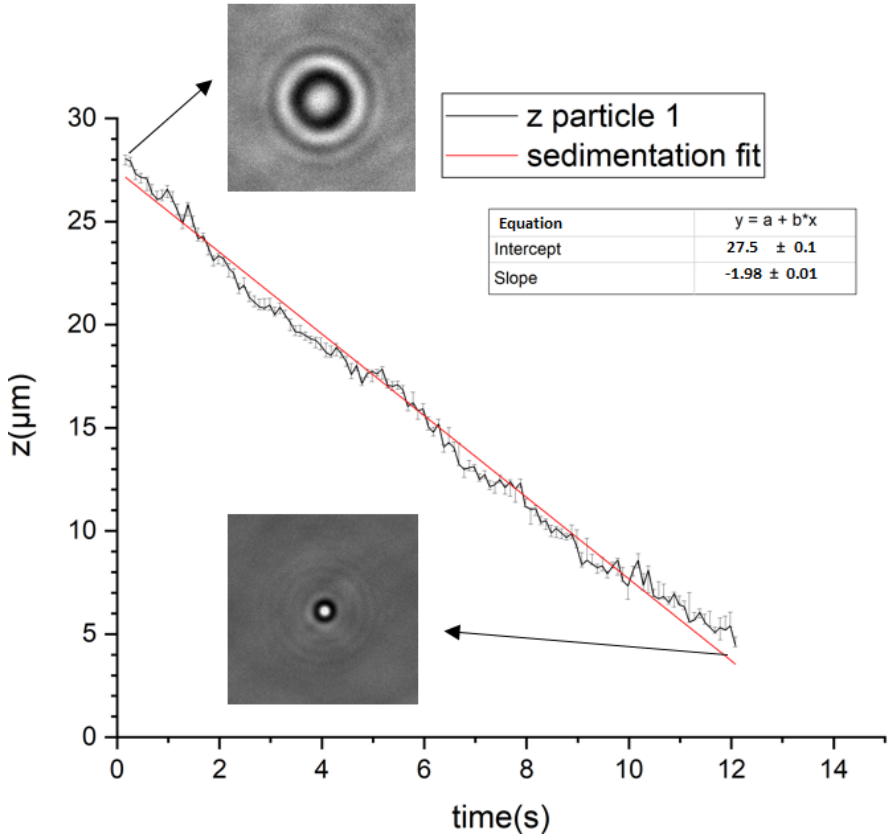

Figure 9: *Trajectory of a silica particle in the z-direction. The focal plane is below the particle as it is sedimenting and hence the stokes velocity is negative. The analysis stops at about 5μm above the focal plane as the Lorenz-Mie scattering model cannot be fitted close to focus. Z positions are shown with the error bars produced by the fitting and the linear fit is also shown(red). The holograms in the starting and finishing position analysed are shown in the figure to emphasize the qualitative difference produced by the change in height.*

motion for lag times up to 1s. The final lag time point contains 12 pairs, sufficient to reduce errors. Each component of the motion should yield the same diffusion coefficient. As shown in *Figures 11-12* that is indeed the case within error. As predicted we measure a slightly higher diffusion coefficient in all components of the motion and as a result at the total diffusion coefficient. The drift is not subtracted completely from the

	$u_{av}(\mu m/s)$	D($\mu m^2/s$)	errD($\mu m^2/s$)
x	0.342	0.26	0.01
y	0.068	0.20	0.01
z	1.980	0.25	0.08
3D	-	0.24	0.08

Table 1: *Experimental diffusion coefficients.*

Version of September 11, 2019– Created September 11, 2019 - 11:12

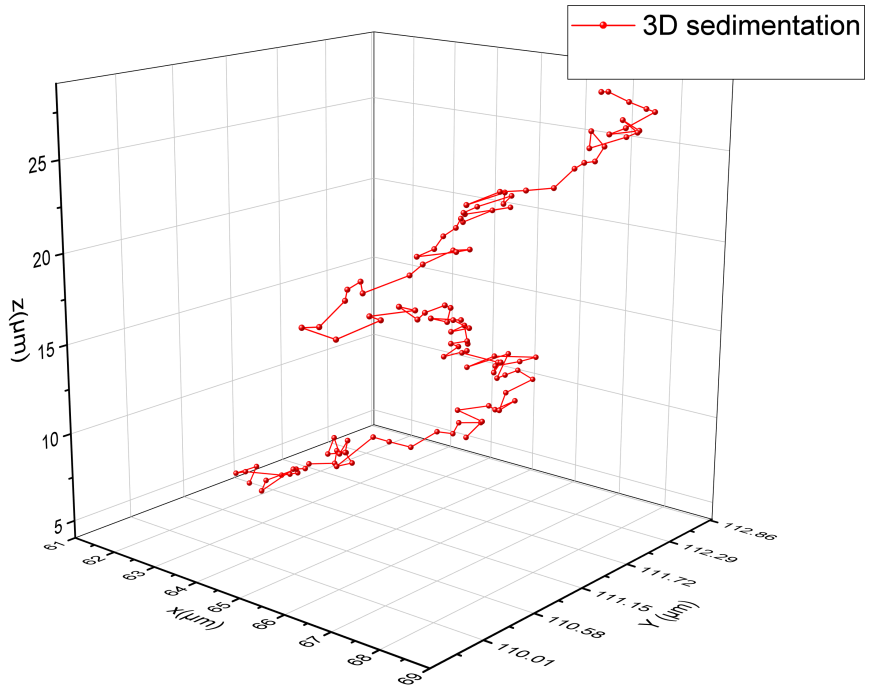

Figure 10: *3D trajectory of a silica particle sedimenting from above the field of view towards focus. Each point is separated by 100ms. The trajectory is dominated by gravity as the Peclet number of this silica particle is 11.*

motion and that could account for the increased value found experimentally.

In *Figures 11-12* the mean square displacement of a single particle is shown. For this trajectory the measured average velocities used for the correction factors are shown in *Table 1* above, as well as the diffusion coefficient D measured, where the correction described by equation (13) has been applied and the subtraction of the sedimentation, and the associated error. The measured values are higher than the theoretical prediction as expected and there is a direct correlation between the size of the average velocity measured due to drift and the increase in D. The diffusion coefficient measured in 3D however is within error in good agreement with the theoretical prediction. We observe a domination of the z-position uncertainty at small lag times, seen in *Figure 12*, which is diminished in larger lag times. This also outlines the limitation of our set-up. We measured diffusion coefficients for a total of 6 trajectories (three pairs) and averaged out the diffusion coefficient that we obtained for the 3D motion of the particle. *Table 2* summarizes the results obtained.

Version of September 11, 2019– Created September 11, 2019 - 11:12

Trajectory	$D_x(\mu m^2/s)$	$D_y(\mu m^2/s)$	$D_z(\mu m^2/s)$	$D(\mu m^2/s)$	errD($\mu m^2/s$)
1	0.26	0.20	0.25	0.24	0.08
2	0.26	0.21	0.26	0.25	0.07
3	0.20	0.21	0.23	0.22	0.08
4	0.21	0.22	0.23	0.22	0.07
5	0.22	0.24	0.24	0.23	0.08
6	0.22	0.22	0.24	0.23	0.08
Avarage	0.23	0.22	0.24	0.23	0.03

Table 2: *Experimentally measured diffusion coefficients for each component of the motion for 6 trajectories. Each pair (i.e. 1-2, 3-4 and 5-6) correspond to 2 halves of a single particle trajectory corresponding to above and below the field of view.*

It is not possible to cross validate our results with previous work as the specification of the particles used varies and changes the diffusion coefficient. We are able, however, to compare the errors we obtain to evaluate the quality of our data. In previous work done by Yevick et. al. (2014) [27] they measured a 10% increased diffusion coefficient compared to the theoretical prediction. After we averaged over all trajectories we obtained a value of $D = 0.23 \pm 0.03 \mu m^2/s$ which is within error in good agreement with the theoretical predictions.

Sedimentation of Janus Spheres

In order to look at the sedimentation of Janus spheres we used the same silica spheres with specifications as in the previous section, with the key difference that one hemisphere was coated with a thin Platinum(Pt) film. The thickness of the platinum film varies, we can however approximate a mean value of $4.7nm$ as given from the internal calibration of the sputtering equipment. The sputtering equipement has an accuracy of 0.1nm for the thickness of the film. Samples were prepared as described in the Method section, and we recorded a series of movies according to the same principles described for the passive silica spheres.

The fitting process for Janus spheres requires a different approach. Due to the nature of the particle there are more parameters one must consider when trying to fit a model to the data. Firstly, the refractive index of platinum films is a complex number, consisting of a real refractive index and an imaginary part, the extinction coefficient. Furthermore, the produced hologram will no longer be symmetric with respect to intensity. As it was shown by Wang et. al. (2014) [28], the orientation of the Pt cap will create asymmetries in the intensity map of the hologram. Thus, compared to our previous analysis, we must consider three extra parameters, the angle of rotation, and the real and imaginary part of the refractive index of platinum.

A literature review revealed that there

Version of September 11, 2019– Created September 11, 2019 - 11:12

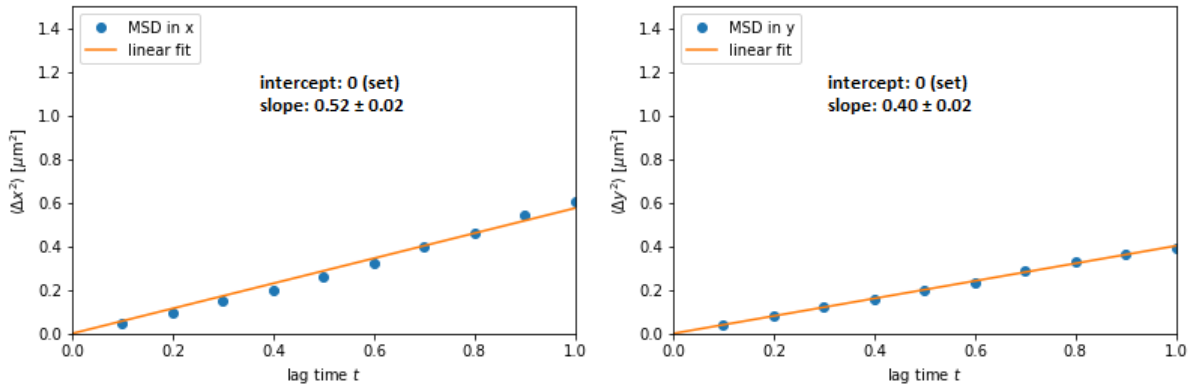

Figure 11: *Mean square displacement calculated for lag times of 1 second for a single silica sphere sedimenting freely in water for the x-y component of the motion.The fit is done with a y-intercept anchor at the axis origin as it is physically expected. The linear relationship confirms the power law and the slope of the fit corresponds to* $2D$.

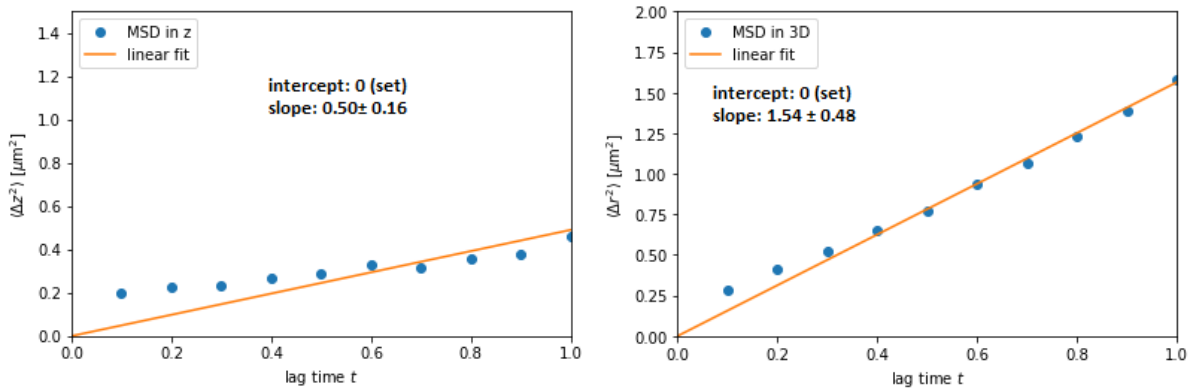

Figure 12: *Mean square displacement calculated for lag times of 1 second for the z component and 3D motion of a silica particle. The slope on the right corresponds to* $6D$. *The discrepancy between fitting and experimental points arise from the dominating uncertainty of the z position at small lag times.*

is no known value for the refractive index of Pt films with thickness of 5nm. It is important to mention that though work has been done on the refractive index of Pt, such as measurements of films by Goddard et. al. (2008) [29], or measurements of wavelength depend transmittance and absorbance by Serbetci et. al. (2014) [30], the thickness of the films discussed is at least two fold the ones that we are using. We note that increasing the thickness of the film is not an option for our experiments as to observe activity we need to maintain the upper

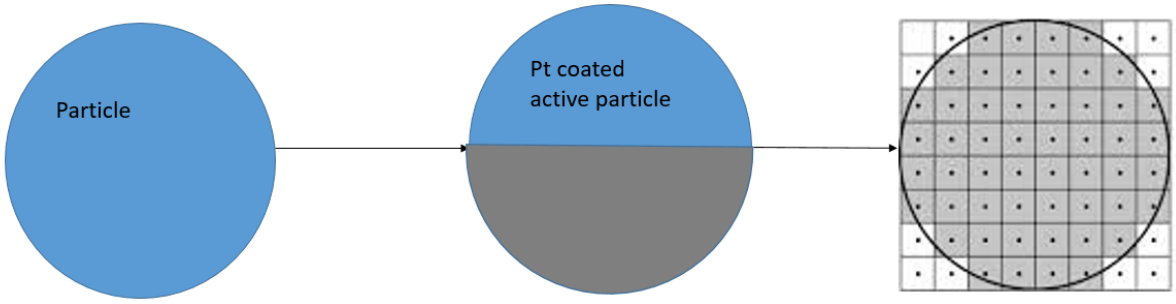

Figure 13: *A schematic showing the discretization of a Janus spheres in scattering dipoles. The top view on the right assumes that the equator of the sphere is perfectly aligned with the focal plane which is rarely true.*

limit of 5nm. Furthermore, the sputtering process with which the spheres are coated is not perfect and it is subject to an equal coating of the hemisphere, as well as fluctuations in the thickness of the cap. With all that in mind, we must employ a numerical approach for calculating the hologram described below.

In order to calculate the scattering field produced by a Janus sphere we must perform a Discrete Dipole Approximation (DDA). The ADDA code[31], which has been developed by the University of Amsterdam and launched as an open source code, performs the required calculations for the scattered field of arbitrary 3D structures and is implemented as an external executable by the Holopy Python library. It comes however, at a high computational cost. As shown in *Figure 13*, the coated scatterer is discretised in a series of dipoles with a composite refractive index. The top view on the left shows an ideal case in which the equator of the Janus sphere is perfectly aligned with the focal plane, therefore the angle of rotation is 0°.

According to the suggestions proposed by the authors [31], there is a minimum of dipoles one must use to obtain a good fit using ADDA. That minimum is defined by the wavelength of illumination and the size of the particles used. The minimum is set at 10 dipoles per wavelength of particle size. For our case of a wavelength of 660nm and particles of radius of 1.06μm, we require a 64000 dipoles (40x40x40) to achieve that minimum. The number of dipoles per direction however must be a power of 2, resulting in a minimum of 64 dipoles per direction. As will be discussed in a later section this approximation is not sufficient to properly approximate a sphere.

Figure 14 is a visual representation of the discretization process of the particle. The sphericity of the discretized particle is reduced as the number of dipoles is reduced, which is a fundamental issue for the fitting as it directly affects the symmetry of the hologram obtained. That issue became a major limiting fac-

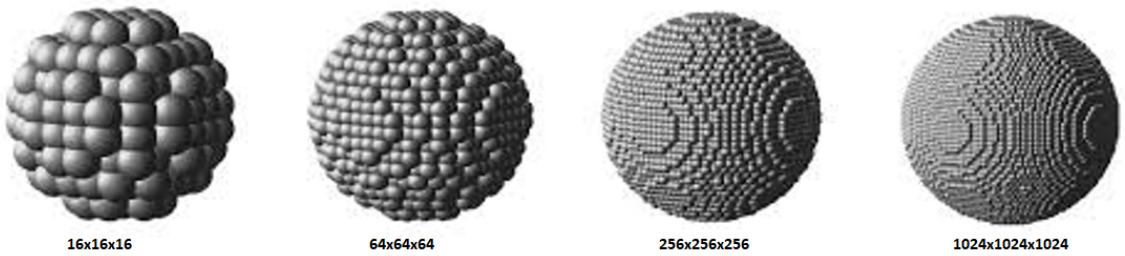

Figure 14: *Discretization of a sphere in a series of dipoles. As it becomes apparent from the schematic the sphericity of the particle is partly lost at low number of particles which results in problems to the fitting process. Image taken from Laczik et. al. (1996)[32]*

tor in any subsequent analysis we attempted to perform as it did not allow us to properly resolve fitting of the active particles (see Discussion).

The enormous computational challenge however arises when the two aforementioned issues are combined. The lack of information about the refractive index in combination with the high number of dipoles results in an high number of parameters which renders the computation impossible with the current tools. Typically, the fitting of a single frame can take up to 2 weeks on an i5 processor with 8GB RAM. With a back of the envelope calculation, it would take about 2 years to analyse a 130 frames movie to obtain a diffusion coefficient. We consider this to be a limiting factor we could not work around with the current microscopy and computational set-up.

Intensity Resolution

We were still interested in the possibilities of our set-up. In particular, we were interested in characterizing at least one Janus sphere in the bulk with respect to its cap rotation. Reviewing previous work by Wang et. al. [28], we looked for the intensity asymmetry created by the rotation of the cap in a hologram. We took a series of images of a Janus sphere coated with 5nm Pt with a 60Xair and 100Xoil objective and then looked at the intensity profile as a heat map. We expected to see an asymmetry in the intensity indicating the position of the cap. Unfortunately, that is not what we observed. Even when averaged over three consecutive frames (rotational diffusion is much slower than 300ms), no intensity asymmetry is present. *Figure 15* shows a heat map of the intensities of the holograms obtained with the 60X air objective. Spikes in the intensity are random around the fringes of the hologram and do not indicate a clear position of the cap. *Figure 16* shows the equivalent heat map of the same particle obtained with the 100X oil objective. The intensity asymmetry is still not visible and hence we conclude that it does not re-

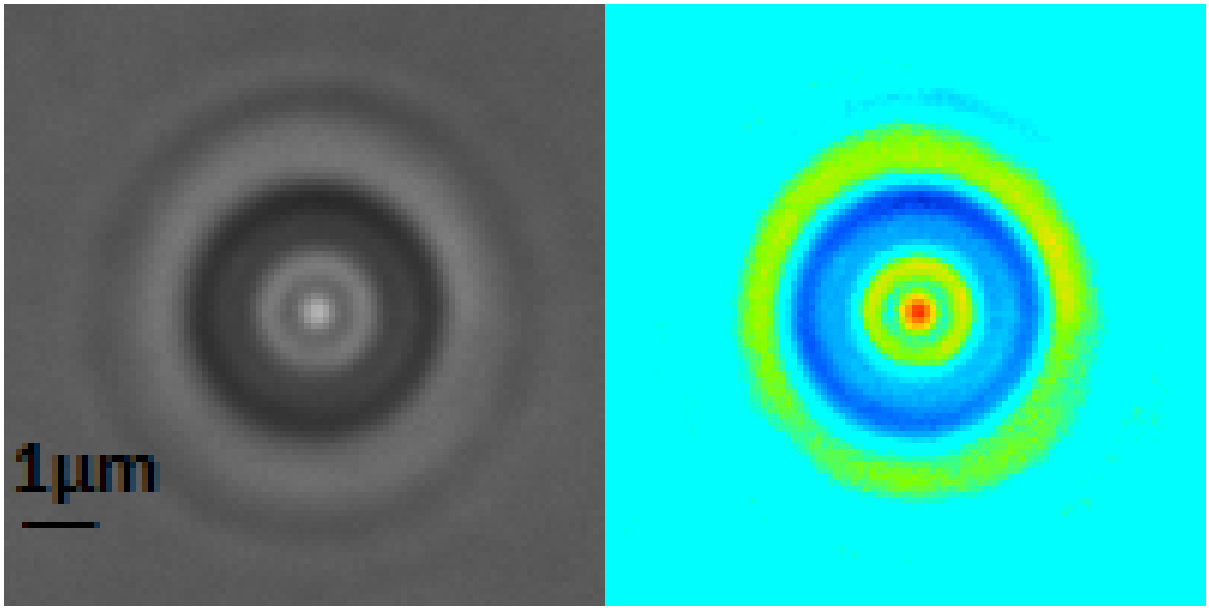

Figure 15: *The intensity map of a Pt-coated colloid. By looking at the heat map of color intensity we notice no visible and consistent assymetry in the fringes' intensity. We believe the intensity does not resolve with our current set-up*

solve.

Discussion

Our results for the diffusion coefficient of the passive spheres appear to be consistent with theory. Previous experiments using similar set-ups [18, 22] have found errors comparable to what we observe from our measurements. It would be possible to further reduce our error by collecting and analysing more trajectories, but even with a sample of 6 trajectories good agreement was achieved. We conclude that inline digital holography is an accurate method for measuring the diffusion coefficient, however, it remains relatively limited with respect to the technical requirements. At this, we mention that the limitation presented by the necessary dilution of the sample to avoid overlapping features and the limited field of view will always pose a difficulty of correcting for the drift of the particles. The use of capillaries would eradicate that issue, however for using active particles it would have posed a series of separate issues due to the H_2O_2. As the fuel is catalyzed bubbles start forming in the sample which interfere severely with the diffraction pattern and render the analysis impossible.

The Baysian inference as a method of analysing the holograms has plenty of advantages but also presents a few disadvantages. Though the fitting is much more accurate and significantly

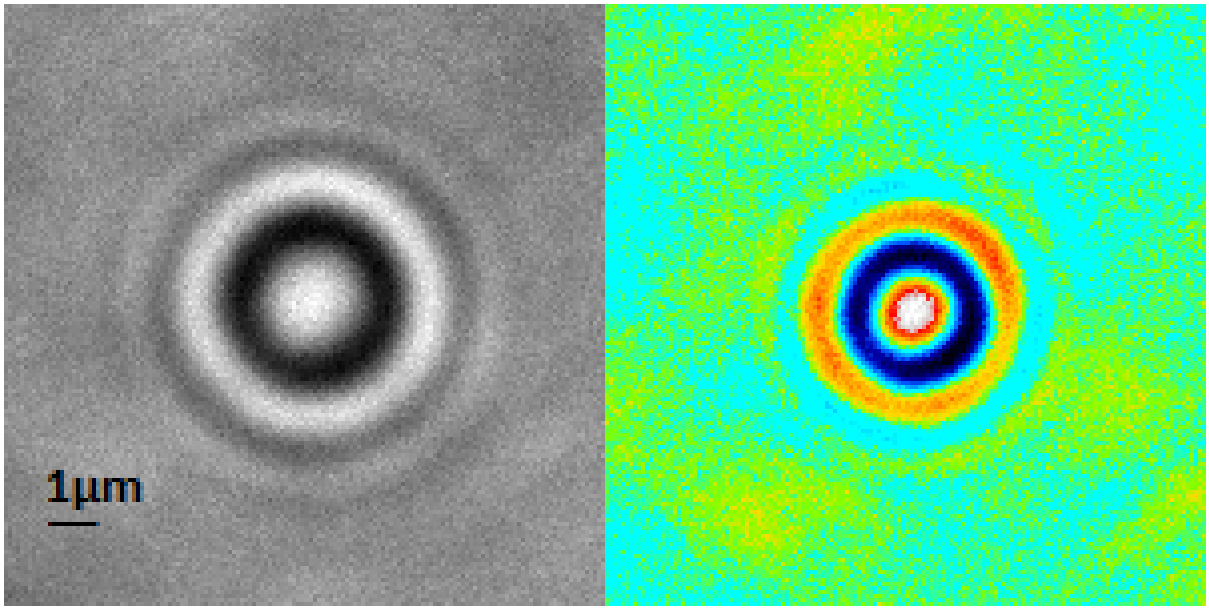

Figure 16: *The intensity map of an Pt-coated colloid. obtained with the 100X oil objective. The asymmetries in the intensity appear random and do not indicate the position of the cap.*

unbiased in comparison to the previously used least square fit, it does depend on the priors given. In addition, initial guesses might yield bad fits and each failed attempt requires a significant amount of time. Though with the passive particles that did not result in a considerable problem, with the Janus spheres it meant that each failed attempt could cost 2 weeks. It is worth considering for the future, the use of a material that can provide both the activity and also has a well measured refractive index, for example TiO_2, as used in previous work [28].

The discrete dipole approximation is the main limiting factor when discussing the possibilities of using digital inline holography for Janus spheres. The enormity of the computational time needed to perform the fitting renders it impractical. Though an excellent technique for characterization of particle properties, which would require less frames to perform, in terms of tracking enough particles to make a strong argument for the motion in the bulk it still remains inefficient. This was the most impact-full factor for our experiments. There are however developments that will in the future allow for a much faster analysis. We mention the work being done by Hannel et. al. (2018) [33] employing a neural network to perform the fitting. It remains a relatively new approach and does not allow for the Janus spheres to be considered but it does show great promise for speeding up the fitting to acceptable time frames. The basic principle employs a pre-trained

network which localizes holograms and starts the fitting generating priors closer to the real parameters of the data. That sort of "memory" of a collection of holograms, allows the network to narrow down the fitting and hence speed it up at a minimal cost of accuracy.

Finally we must address the quality of our set-up, and in particular the coherence of our light source. Though the low temporal coherence of the LED reduces speckle in the holograms, the low spatial coherence reduces the sharpness and results in the resolution of less fringes than what is obtained with a laser source. We believe that the resolution of the asymmetry in intensity that should be present in Janus spheres would be resolved if we used a more coherent source. In addition, with the use of optical tweezers we can perform a characterization of a particle with a known z-position, offering a way to tackle the unknown parameter of the refractive index. It would also allow us to provide better priors for the z-position when tracking a particle. Furthermore, a more coherent source yields more fringes, which directly relates to how accurate the fitting is, reducing our errors further.

Conclusion

Digital Inline Holography as a tool to track active colloidal particles and measure their diffusion coefficient in the bulk remains a difficult problem to solve. Our attempts described in this project yield some promising results and point out to a series of improvements in order to approach the problem. Through trial and error we have managed to optimize a series of aspects of the technique to fit our requirements but there is still things that need to be considered.

We managed to correctly measure the diffusion coefficient of silica spheres in the bulk of the medium using an affordable set-up both for the microscope and computations. Partially achieving the goal set out by this project did not only showed us the necessary improvements but also revealed the possibilities of this techniques when applied to colloids.

Aknowledgements

A thank you to the Soft Matter Group of Leiden University for the opportunity and the provision of the equipment for this research project. To Dr. Daniela Kraft for her guidance. To Ruben Verweij for his endless patience and excellent supervision. To Stefania Ketzetzi for always pointing to the most relevant publications. And to Rachel Doherty for always making sure no-one burns down the lab.

Bibliography

[1] R. W. Perry, G. Meng, T. G. Dimiduk, J. Fung, and V. N. Manoharan, *Real-space studies of the structure and dynamics of self-assembled colloidal clusters*, Faraday Discuss. **159**, 211 (2012).

[2] V. D. Nguyen, S. Faber, Z. Hu, G. H. Wegdam, and P. Schall, *Controlling colloidal phase transitions with critical Casimir forces*, Nature Communications **4**, 1584 EP (2013), Article.

[3] J. Fung, K. E. Martin, R. W. Perry, D. M. Kaz, R. McGorty, and V. N. Manoharan, *Measuring translational, rotational, and vibrational dynamics in colloids with digital holographic microscopy*, Opt. Express **19**, 8051 (2011).

[4] V. N. Manoharan, *Colloidal matter: Packing, geometry, and entropy*, Science **349** (2015).

[5] R. J. Price, D. M. Skyba, S. Kaul, and T. C. Skalak, *Delivery of Colloidal Particles and Red Blood Cells to Tissue Through Microvessel Ruptures Created by Targeted Microbubble Destruction With Ultrasound*, Circulation **98**, 1264 (1998).

[6] A. Tsyrenova, K. Miller, J. Yan, E. Olson, S. M. Anthony, and S. Jiang, *Surfactant-Mediated Assembly of Amphiphilic Janus Spheres*, Langmuir **35**, 6106 (2019).

[7] L.-T.-C. Tran, S. Lesieur, and V. Faivre, *Janus nanoparticles: materials, preparation and recent advances in drug delivery*, Expert Opinion on Drug Delivery **11**, 1061 (2014), PMID: 24811771.

[8] Y. Nonomura, S. Komura, and K. Tsujii, *Surface-Active Particles with Microstructured Surfaces*, Langmuir **21**, 9409 (2005).

[9] L. S. Palacios, J. Katuri, I. Pagonabarraga, and S. SÃ¡nchez, *Guidance of active particles at liquid liquid interfaces near surfaces*, Soft Matter **15**, 6581 (2019).

[10] A. Carpio, T. Dimiduk, V. Selgas, and P. Vidal, *Optimization Methods for In-Line Holography*, SIAM Journal on Imaging Sciences **11** (2018).

[11] S.-H. Lee, Y. Roichman, G.-R. Yi, S.-H. Kim, S.-M. Yang, A. van Blaaderen, P. van Oostrum, and D. G. Grier, *Characterizing and tracking single colloidal particles with video holographic microscopy*, Opt. Express **15**, 18275 (2007).

[12] G. Gouesbet, *Generalized lorenz-mie theory and applications*, Particle & Particle Systems Characterization **11**, 22 (1994).

[13] X. Fan, W. Zheng, and D. J. Singh, *Light scattering and surface plasmons on small spherical particles*, Light: Science &Amp; Applications **3**, e179 EP (2014), Review.

[14] Ondarçuhu, T., Fabre, P., Raphaël, E., and Veyssié, M., *Specific properties of amphiphilic particles at fluid interfaces*, J. Phys. France **51**, 1527 (1990).

[15] R. F. Ismagilov, A. Schwartz, N. Bowden, and G. M. Whitesides, *Autonomous Movement and Self-Assembly*, Angewandte Chemie International Edition **41**, 652 (2002).

[16] G. Volpe, I. Buttinoni, D. Vogt, H.-J. KÃŒmmerer, and C. Bechinger, *Microswimmers in patterned environments*, Soft Matter **7**, 8810 (2011).

[17] M. Khorasaninejad, A. Ambrosio, P. Kanhaiya, and F. Capasso, *Broadband and chiral binary dielectric meta-holograms*, Science Advances **2** (2016).

[18] T. Dimiduk and V. N. Manoharan, *Bayesian approach to analyzing holograms of colloidal particles*, Optics Express **24**, 24045 (2016).

[19] J. Goodman and J. Weare, *Ensemble samplers with affine invariance*, Communications in Applied Mathematics and Computational Science, Vol. 5, No. 1, p. 65-80, 2010 **5**, 65 (2010).

[20] D. Foreman-Mackey, D. W. Hogg, D. Lang, and J. Goodman, *emcee: The MCMC Hammer*, Publications of the Astronomical Society of the Pacific **125**, 306 (2013).

[21] C. van der Wel, R. K. Bhan, R. Verweij, H. C. Frijters, Z. Gong, A. D. Hollingsworth, S. Sacanna, and D. Kraft, *Preparation of Colloidal Organosilica Spheres through Spontaneous Emulsification*, Langmuir **33** (2017).

[22] M. Hannel, C. Middleton, and D. G. Grier, *Holographic characterization of imperfect colloidal spheres*, Applied Physics Letters **107**, 141905 (2015).

[23] A. van Blaaderen, J. Peetermans, G. Maret, and J. Dhont, *Long-time self-diffusion of spherical colloidal particles measured with fluorescence recovery after photobleaching*, The Journal of Chemical Physics **96**, 4591 (1992).

[24] F. C. Cheong, P. Kasimbeg, D. B. Ruffner, E. H. Hlaing, J. M. Blusewicz, L. A. Philips, and D. G. Grier, *Holographic characterization of colloidal particles in turbid media*, Applied Physics Letters **111**, 153702 (2017).

[25] Y. Deng and D. Chu, *Coherence properties of different light sources and their effect on the image sharpness and speckle of holographic displays*, Scientific Reports **7**, 5893 (2017).

[26] X. Michalet, *Mean square displacement analysis of single-particle trajectories with localization error: Brownian motion in an isotropic medium*, Physical review. E, Statistical, nonlinear, and soft matter physics **82**, 041914 (2010), 21230320[pmid].

[27] A. Yevick, M. Hannel, and D. G. Grier, *Machine-learning approach to holographic particle characterization*, Opt. Express **22**, 26884 (2014).

[28] A. Wang, T. G. Dimiduk, J. Fung, S. Razavi, I. Kretzschmar, K. Chaudhary, and V. N. Manoharan, *Using the discrete dipole approximation and holographic microscopy to measure rotational dynamics of non-spherical colloidal particles*, Journal of Quantitative Spectroscopy and Radiative Transfer **146**, 499 (2014), Electromagnetic and Light Scattering by Nonspherical Particles XIV.

[29] L. Goddard, K. Y. Wong, A. Garg, E. Behymer, G. Cole, and T. Bond, *Measurements of the complex refractive index of Pd and Pt films in air and upon adsorption of H2 gas*, in *LEOS 2008 - 21st Annual Meeting of the IEEE Lasers and Electro-Optics Society*, pages 569–570, 2008.

[30] Z. Serbetci, B. Gunduz, A. Al-Ghamdi, F. Al-Hazmic, K. Arik, P. F. El-Tantawy, F. Yakuphanoglu, and A. Farroq, *Determination of Optical Constants of Nanocluster CdO Thin Films Deposited by Sol-Gel Technique*, Acta Physica Polonica A **126**, 798 (2014).

[31] M. Yurkin and A. Hoekstra, *The discrete-dipole-approximation code ADDA: Capabilities and known limitations*, Journal of Quantitative Spectroscopy and Radiative Transfer **112** (2011).

[32] Z. Laczik, *Discrete-dipole-approximation-based light-scattering calculations for particles with a real refractive index smaller than unity*, Appl. Opt. **35**, 3736 (1996).

[33] M. D. Hannel, A. Abdulali, M. O'Brien, and D. G. Grier, *Machine-learning techniques for fast and accurate feature localization in holograms of colloidal particles*, Opt. Express **26**, 15221 (2018).